Journal of Cleaner Production 479 (2024) 143997

Contents lists available at ScienceDirect

Journal of Cleaner Production

journal homepage: www.elsevier.com/locate/jclepro

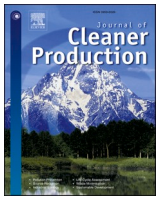

Modeling the health impact of wastewater contamination events in drinking water networks

Sotirios Paraskevopoulos [a,b,*], Stelios Vrachimis [c,d], Marios Kyriakou [c], Demetrios G. Eliades [c], Patrick Smeets [a], Marios Polycarpou [c,d], Gertjan Medema [a,b]

[a] KWR Water Research Institute, Groningenhaven 7, P.O. Box 1072, 3430, BB Nieuwegein, the Netherlands
[b] Department of Water Management, Delft University of Technology, Stevinweg 1, 2628, CN Delft, the Netherlands
[c] KIOS Research and Innovation Center of Excellence, University of Cyprus, Cyprus
[d] Department of Electrical and Computer Engineering, University of Cyprus, Cyprus

ARTICLE INFO

Handling Editor: Zhen Leng

Keywords:
QMRA
Wastewater contamination
Drinking water network modeling
Pathogens
EPANET-MSX

ABSTRACT

Pathogen intrusion in drinking water systems can pose severe health risks. To better prepare in planning and responding to such events, computational models that capture the intrusion and health impact dynamics are needed. This study presents a novel benchmark testbed that integrates current knowledge on pathogen transport and fate in chlorinated systems and can assess infection risk from contamination events. The model considers organic matter degradation, chlorine decay mechanisms, pathogen inactivation kinetics, as well as stochastic water demands.

We studied modeling of wastewater intrusion events that can occur anywhere within a chlorinated and non-chlorinated network. We applied the *Quantitative Microbial Risk Assessment* framework focusing on three pathogens: enterovirus, *Campylobacter*, and *Cryptosporidium*, and their respective dose-response models. Synthetic household-level water demand time series were used to model the individual water consumption timing and calculate the infection risk (exposure via ingestion).

Model outcomes indicate that while chlorination aids mitigation, larger contaminations can still lead to infections due to chlorine resistance (for *Cryptosporidium*) and chlorine depletion at the contamination point. In our example scenarios, chlorine-susceptible pathogens infected 0.78 –26.6 % of the downstream population, while chlorine-resistant ones infected the entire downstream population. Enterovirus infection risk is higher, despite the concentrations in the contamination source being lower, due to the lower susceptibility to chlorine than *Campylobacter*. In non-chlorinated networks, the modeled wastewater contamination events led to 11 –46 % infection risk in the total population, depending on the contamination location. Hydraulic uncertainty had a limited influence on infection risk. Furthermore, *Campylobacter's* infection risk is more sensitive to the initial concentration in the contamination source whereas enterovirus infection risk to the inactivation rate. The model further indicates that the time window for effective mitigation of the magnitude of a waterborne outbreak is short (within hours).

1. Introduction

Safe drinking water is crucial for society, impacting health and well-being. Drinking water distribution networks (DWDN) are critical infrastructures, recognized by USA's Presidential Policy Directive 21 and the European Union's Directive (EU) 2022/2557. This requires plans to enhance water suppliers' resilience against natural, accidental, and malicious threats (Teixeira et al., 2019). One such threat is wastewater intrudes into the DWDN. This can expose thousands to contaminated tap water, causing acute health effects from pathogens (Hrudey and Hrudey,

Abbreviations: DWDN, Drinking Water Distribution Network; QMRA, Quantitative Microbial Risk Assessment; TOC, Total Organic Carbon; BattLeDIM, Battle of the Leakage Detection and Isolation Method; STREaM, Stochastic Residential water End-use Model; CRA, Chlorine-reducing agents; NOM, Natural Organic Matter; SRA, Slow chlorine-reducing agents; FRA, Fast chlorine-reducing agents; CFU, Colony Forming Units; PFU, Plaque forming units; BeWaRE, Benchmark for Water network and Risk Evaluation.

* Corresponding author. KWR Water Research Institute, Groningenhaven 7, P.O. Box 1072, 3430, BB Nieuwegein, the Netherlands.
E-mail address: S.Paraskevopoulos@tudelft.nl (S. Paraskevopoulos).

https://doi.org/10.1016/j.jclepro.2024.143997
Received 24 January 2024; Received in revised form 10 October 2024; Accepted 14 October 2024
Available online 18 October 2024

2004). Proper DWDN operation and maintenance ensures hygiene and hydraulic integrity, preventing pathogen intrusion (Medema et al., 2013). In systems with residual disinfectants, high disinfectant concentration can maintain safety when standard conditions are not met (Lechevallier, 1999). However, outbreaks have been linked to fecal contamination in (chlorinated) networks, often due to cross-connection between sewage- and drinking-water pipelines or intrusion during main breaks (Craun and Calderon, 2001; Hrudey and Hrudey, 2019). Specifically, van Lieverloo et al., 2007) note that 26% of the outbreaks in the UK from 1911 to 1995 were caused by failures in the DWDN. Additionally, 18–20% of outbreaks in Nordic countries from 1975 to 1991 and 18% of outbreaks in the USA from 1971 to 1998 were attributed to similar failures. Notable incidents such as the wastewater contamination in Nokia, Finland with 8453 cases (Laine et al., 2011), or the wastewater infiltration events in Italy (Giammanco et al., 2018) and in Denmark (Kuhn et al., 2017) resulting in 25 and 63 cases respectively, highlight the vulnerability of those systems to contamination. During a contamination event, authorities must assess health impacts and respond quickly and effectively. Accurate representation of contamination type and site, demand-driven hydraulics, understanding of contaminant transport, and the effect of a residual disinfectant as a mitigation are crucial for a comprehensive assessment and rapid, efficient response.

An approach to assess the risk during contamination in the DWDN is to perform a Quantitative Microbial Risk Assessment (QMRA). This estimates customers' exposure to enteric pathogens through ingestion. Studies have combined hydraulic modeling and QMRA for evaluating health risks after wastewater intrusion in DWDNs. For instance, Teunis et al. (2010) examined the risk of norovirus intrusion from sewers into DWDNs due to negative pressure transients. They used the EPANET-MSX hydraulic model and Monte Carlo simulations for random virus entry and dilution estimation. Their study considered the coincidence of virus presence and tap water usage, finding that this factor significantly affects the calculated infection risk level and distribution in the population. Another effort described by Yang et al. (2011) involved surge modeling and hydraulic simulations to model a virus intrusion in a DWN again due to pressure transients. The authors employed EPANET-MSX to integrate a Chick-Watson model that accounted for the inactivation kinetics of selected pathogens and chlorine decay. They concluded that the factors influencing the risk of viral infection were the duration of the negative pressure event and the number of affected nodes, without incorporating stochastic water demand or other water quality parameters. Blokker et al. (2018) developed a QMRA model for contamination events after main repairs in non-chlorinated DWDNs. They discovered that pathogen concentration greatly influences the ingested dose and that the infection risk varies notably between pathogens due to different dose-response relationships.

Controlling pathogens in the DWDN heavily relies on residual disinfectants. Over the past 25 years, there's been increasing interest in modeling chlorine (Cl) transport and decay due to reactions with total organic carbon (TOC) in DWDNs. Frankel et al. (2023) assessed the uncertainty of drinking water quality in DWDNs, specifically focusing on monochloramine decay. They focused on quantifying the effects of hydraulic and chemical uncertainties on water quality predictions. They conducted a sensitivity analysis and Monte Carlo simulations to identify the most influential chemical parameter and explore the impact of both chemical and hydraulic uncertainty. Their findings were that monochloramine uncertainty is significantly influenced by hydraulic variability and increases as water age increases. Their study emphasized the importance of accounting for these uncertainties to make accurate model-based decisions for managing water quality in DWDNs. Pelekanos et al. (2021) applied a parallel first-order bulk and wall chlorine decay model to evaluate a network's vulnerability to deliberate contamination attacks, using nominal water demands. They found that contamination location significantly affects the size of the exposed population. Abhijith and Ostfeld (2021) examined a chlorinated (and chloraminated) network's response to arsenic contamination using second-order kinetics, based on competing reactions in water. This study emphasized the critical role of disinfectant residual. Lastly, Fisher et al. (2017a) used a two-reactant model with fast and slow agents, incorporating temperature as it greatly affects bulk chlorine decay. Eliades et al. (2023) provided a detailed review of contamination event diagnosis tools, emphasizing the need for realistic physical and virtual testbeds to simulate contamination emergencies and assess their impact, considering uncertainties. However, most models use generic contamination approaches, lacking tools to accurately represent pathogen dynamics-and failing to consider all important modeling parameters together. To the best of the author's knowledge, there has not been any other attempt to model all the different reactions that occur in a DWDN simultaneously during a wastewater contamination event, while also using stochastic water demands and assessing the infection risk using QMRA.

In line with this, to enable responsible authorities to prepare for and respond effectively to contaminations, we have developed a novel, open benchmark testbed named BeWaRE (Benchmark for Water network and Risk Evaluation). This testbed integrates all current relevant knowledge regarding the transport and fate of pathogens in chlorinated systems in one model and is capable of estimating the health impacts of such events. With BeWaRE, responsible authorities can model various contamination events. These events vary from minor, where negative pressure transients cause slight wastewater entry, to major accidents with significant wastewater influx. The benchmark can be used for developing new software and decision support tools for monitoring, control, and management of contamination emergencies, as well as creating datasets for machine learning research.

BeWaRE integrates the findings of previous studies, accounting for bulk and wall chlorine decay, various pathogen inactivation kinetics, TOC degradation, and realistic water demands and consumption distribution, incorporating QMRA.

The contributions of this work are summarized below:

- Introduction of an open-access testbed designed for comprehensive simulation of contamination by waterborne pathogens under various disinfection regimes.
- Integration of realistic household consumption profiles improving daily consumption pattern accuracy and health impact calculations for waterborne pathogens using QMRA.
- Investigation of a wastewater contamination event and evaluation of the importance of the input parameters.

Specifically, this paper presents a benchmark hydraulic and water-quality model to assess the health impact following a large wastewater contamination in a chlorinated and non-chlorinated network and evaluate chlorine's mitigating effect. The model was tested using a modified version of L-Town, a benchmark network from the BattLeDIM (Battle of the Leakage Detection and Isolation Methods) competition (Vrachimis et al., 2022), featuring 782 junctions, 905 pipe segments, and serving approximately 28,000 citizens. In our example, we investigated a single contamination event originating from three distinct locations using *Campylobacter*, enterovirus, and *Cryptosporidium* as reference pathogens. Hydraulic uncertainty was addressed to account for the dynamic, uncertain nature of water demands and examine their influence on the model outcome. Water quality uncertainty was included to examine the effects of variability of input parameters on the model outcome. The model outcome is the expected health impact over time and space, expressed as the expected number of infections, and the infection risk, following the QMRA steps.

2. Benchmark model development

The benchmark model developed is depicted in Fig. 1. The hydraulic modeling includes stochastic water demands that determine the hydraulics of the entire network. This involves modeling different water end-uses, from which we isolate the tap water end-use. As shown in the

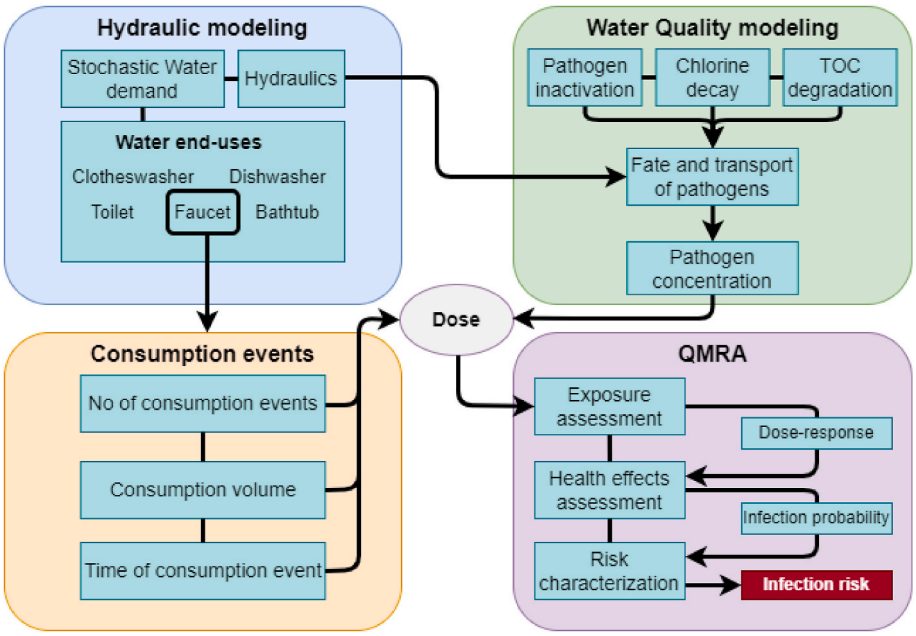

Fig. 1. The flowchart of BeWaRE model with the integration of all components.

figure, we generate individual tap water consumption events that will later be used for the risk assessment. The hydraulic modeling is also integrated with the water quality modeling component. The water quality modeling includes simulating reactions between different agents of interest, eventually leading to the calculation of pathogen concentration. This concentration, combined with the volume calculated from the consumption events, is used to determine the dose. The dose is then integrated into the QMRA part to assess the infection risk. All the different components of the BeWaRE model are described in detail in the following chapters.

2.1. Network graph

The topology of the DWDN is modeled by a directed graph denoted as $\mathscr{G} = (\mathscr{V}, \mathscr{E})$. Here, $\mathscr{V}$ is the set of nodes such that $\mathscr{V} \subset Z \times \Theta_v$. The set $Z = \{1, \cdots, n_v\}$ indicates the positive integers representing the index of the i-th node, $v_i \in \mathscr{V}$, and $|\mathscr{V}| = n_v$ is the total number of nodes. Nodes represent pipe junctions and consumer (water demand) locations, reservoirs, and tanks. The set Θ_v associates each node with parameters (real numbers) detailing the network's physical properties that affect water flow and quality, such as node elevation. Each node v_i is associated with a time-varying consumer water demand, denoted by $d_i(t)$. The set $\mathscr{E}$ represents edges (links) defined as $\mathscr{E} \subset \mathscr{V} \times \mathscr{V} \times \Theta_e$. An edge $e_{(i,j)} \in \mathscr{E}$ connects nodes v_i and v_j where $i, j \in Z$ and $i \neq j$. The total link count is $|\mathscr{E}| = n_e$. Links represent pipes, pumps, and valves, with pumps and valves being the main hydraulic control elements in a DWDN. The set Θ_e associates the edge with its parameters (real numbers). Depending on the edge type, parameters vary. For instance, a pipe might have length, diameter, and roughness as parameters, while a pump's parameters might be polynomial coefficients defining its characteristic curve. In this work, both Θ_v and Θ_e parameters are considered time-invariant since they refer to characteristics of pipes and nodes that may change slowly over time (e.g., years), while we consider wastewater contamination events lasting from hours to days.

2.2. Consumer demand modeling

The main driver of water network hydraulics is consumer demand at nodes, represented as $d_i(t)$ for the time-varying demand at node v_i. Typically, demand is modeled by an average or base demand component, multiplied by a daily or weekly consumption pattern. Approximations of base demand data can be deduced from the utility's billing records, while patterns are usually rough approximations (Vrachimis et al., 2019). We employ the *STochastic Residential water End-use Model* (STREaM) tool, to generate synthetic household-level water demand time series. STREaM uses a large dataset with observed and disaggregated water end-uses from over 300 single-family U.S households (Cominola et al., 2018). The associated water end-uses are toilet, faucet, bathtub, clothes washer, and dishwasher. Each water end-use has distinct consumption patterns and probability distributions for water use volume, use duration, daily frequency, and time of use during the day. This gives a realistic residential demand profile for the L-Town network, ignoring non-residential demands such as industries. To derive a daily demand time-series $d_i(t)$ per node, we use the L-Town network's base demand to calculate the population associated to node v_i, defined as $Pop_{(i)}$, assuming an average consumption of 150 L/day per person. Multiple simulations of the STREaM tool are employed with different household occupancy to allow for variations in consumption patterns until the total occupancy equals $Pop_{(i)}$. The demand profile for node v_i, indicated by $d_i(t)$, is the combined household consumption at each time instant. Note that, using this demand modeling approach, different daily tap water end-uses per individual can be distinguished at each node and used in the exposure assessment (part of QMRA as discussed in chapter 3).

2.3. Hydraulic dynamics

The key hydraulic quantity associated with each node v_j is the *hydraulic head*, denoted by h_j. The main hydraulic quantity associated with a link $e_{(i,j)}$ is the *water flow*, denoted by $q_{(i,j)}$ (Boulos et al., 2006). The overall hydraulic state $x^h \in R^{n_h}$ of a DWDN is defined by the head at nodes and flow in links, thus $n_h = n_v + n_e$. These states are calculated using a hydraulic model of a DWDN, which is a set of equations derived from the laws of (i) conservation of mass; and (ii) conservation of energy in the network. In this work, we use the EPANET modeling software (Rossman, 2000) to solve these equations, which uses the *pipe formulation* as proposed by Todini (1987).

2.4. Water-quality dynamics

Water quality characterizes the concentration of key variables in water, while water quality dynamics describes changes in the concentration of physical, chemical, and biological agents within the DWDN over time and space. Agents in a DWDN either react with others altering concentrations over time or maintaining a constant concentration. Both types of agents are diluted and transferred within the water, thus their concentration at a particular network location changes over time.

Let $W \in R^{n_w}$ be a vector indicating the concentration of n_w agents of interest in a DWDN, at a certain location and time, with $w^{(i)}$ being the i-th agent. We focus on certain agents because they either need to be controlled or because they may react with these controlled agents.

Reaction dynamics explain how agent concentrations change due to reactions or decay. Single-species reaction dynamics, commonly used in water quality modeling literature, describe the decay rate of an agent (Clark et al., 2010), representing the concentration of a single agent, $w^{(i)}$, while neglecting others. This simplification is convenient since we typically don't know all reactions and agents present in water.

During normal operation, hydraulic dynamics in a water network influence the water quality dynamics through agent transport along pipes and dilution at pipe junctions. The change in agent concentration over time t and space, coupled with reaction dynamics in bulk water and on pipe surfaces (axial dispersion neglected for simplicity), is represented by a first-order hyperbolic partial differential equation (Eliades et al., 2023):

$$\frac{\partial W_{(i,j)}(z,t)}{\partial t} + \frac{q_{(i,j)}(t)}{\alpha_{(i,j)}} \frac{\partial W_{(i,j)}(z,t)}{\partial z} = f_r\left(W_{(i,j)}(z,t), \Theta_r\right) + B(z)u_{(i,j)}(z,t) + B(z)\phi_{(i,j)}(z,t) \quad (1)$$

where $W_{(i,j)}(z,t)$ is the agent concentrations vector in water at continuous time t and at distance z along a pipe corresponding to the edge $e_{(i,j)}$, with water flow $q_{(i,j)}(t)$ and pipe cross-sectional area $\alpha_{(i,j)} \in \Theta_e$. The function $f_r(\cdot)$ denotes concentration changes due to reactions with other agents in the water or on pipe walls, considering the pipe parameter vector Θ_r. The function $u_{(i,j)} \in R^{n_w}$ represents controlled agent input (e.g., disinfectant addition). The function $\phi_{(i,j)}(z,t) \in R^{n_w}$ corresponds to the uncontrolled injection of contaminants that can occur at any location in a DWDN (e.g., wastewater intrusion). The matrix $B(z)$ specifies the injection location and agent type. Note that, if a new agent is added to the network, this needs to be included in W, and suitably modify function $f_r(\cdot)$ if this reacts with other agents.

In general, this hyperbolic partial differential equation cannot be solved analytically, however, a numerical solution is possibly by using a suitable discretization method. One approach is to segment the network into finite volumes, and model multi-species reactions (Shang et al., 2008a) as coupled sets of differential and algebraic equations solved for each finite volume of the network, summarized by:

$$\frac{dW(t)}{dt} = f_r(W(t), \Theta_r) \quad (2)$$

$$f_g\left(W(t), \Theta_g\right) = 0 \quad (3)$$

where W is a vector of average concentrations of n_w agents of interest within a finite volume, $f_r(\cdot)$ is a vector field denoting concentration change due to decay reactions between agents, $f_g(\cdot)$ corresponds to the algebraic equations for mass balance, and Θ_r, Θ_g are the coefficients of the reaction kinetics.

In this work, we used EPANET for the hydraulic modeling and EPANET-MSX for multi-reaction modeling, chosen for their open-source tool ecosystem, for instance, the EPANET-MATLAB Toolkit for effective scenario simulations in MATLAB (Eliades et al., 2016). Regarding advection dynamics, this benchmark model employs the EPANET-MSX simulator with the following core assumptions:

a) Advective transport in pipes: agents move with the fluid's average velocity and interact with other species and pipe walls.
b) Mixing at pipe junctions: Inflows from multiple links are assumed to mix completely and instantly.
c) Mixing in storage nodes: all inflows to tanks mix completely with existing contents, subject to possible bulk phase reactions, with alternative schemes available to model plug flow.

2.5. Agents of interest during wastewater intrusion

Water quality dynamics largely depend on the chosen agents W and the differential equations $f_r(\cdot)$ that describe their reactions. For example, contaminants may react with disinfectants, reducing disinfectant concentration.

Table 1 lists the reference pathogens that were modeled, each representing a pathogen group (bacterium, virus, protozoon) with varying Cl resistance and infectivity. The selection of these pathogens is primarily due to their frequent occurrence in wastewater, differences in chlorine resistance, and high infectivity. Their data availability and use in existing literature, offers a comparative and well-established basis for their inclusion in our analysis (Betanzo et al., 2008; Laine et al., 2011; Odhiambo et al., 2023). For modeling, we denote pathogens as the agents of interest, represented by $w^{(1)} = C_P$ (organisms /L). They enter drinking water during a large wastewater intrusion event, i.e., the first contaminant input $\phi^{(1)} = P$ (organisms).

Cl (mg) is a key agent of interest, as it impacts pathogen concentration. We denote the concentration of chlorine as $w^{(2)} \equiv C_{Cl}$ (mg /L), while the injected concentration of chlorine is a controlled input $u^{(1)} \equiv C_{Cl}$ (mg /L). Wastewater carries organic and inorganic compounds reacting with chlorine in a chlorinated network. We designated TOC as an indicator of all chlorine-reducing agents (CRA) in water that includes both Natural Organic Matter (NOM), typically considered as slow chlorine-reducing agents (SRA), and the inorganic compounds (such as ammonia and iron), that are typically fast chlorine-reducing agents (FRA), as seen in other studies (Vieira et al., 2004; Monteiro et al., 2014; Fisher et al., 2017a). The use of TOC as an indicator is convenient since it is measurable, however, it is important to note that not all TOC contributes directly to chlorine demand, since it includes both reactive and non-reactive compounds. FRA and SRA from wastewater are denoted by $w^{(3)} \equiv C_{FRA}$(mgCl-equiv /L), $w^{(4)} \equiv C_{SRA}$(mgCl-equiv /L), and modeled as contamination inputs $\phi^{(2)} \equiv FRA$ (mgCl-equiv), $\phi^{(3)} \equiv SRA$ (mgCl-equiv). CRA is found at lower levels in drinking water than in wastewater and mostly consists of SRA. We account for this by inserting additional SRA at DWDN entry points, denoted by $u^{(2)} \equiv C_{SRA}$(mgCl-equiv /L).

The complete state, control input, and contamination input vectors for this benchmark model are then given by:

$$W = [C_P, C_{Cl}, C_{FRA}, C_{SRA}]^\top, U = [C_{Cl}, C_{SRA}]^\top, \Phi = [P, FRA, SRA]^\top \quad (4)$$

2.6. Modeling reactions

The water quality dynamics cover concentrations of four agents: Chlorine C_{Cl} (mg/L), fast and slow reducing agents C_{FRA}, C_{SRA} (mgCl-equiv/L), and various reference pathogens C_{P_i} in Colony Forming Units (CFU/L), plaque-forming units (PFU/L) and oocysts/L, all assumed

Table 1
Waterborne pathogens and their significance in water supplies. Adapted from WHO. Guidelines for drinking water quality (World Health Organization, 2017).

Pathogen	Health significance	Persistence in water supplies	Chlorine resistance	Relative infectivity
Campylobacter	High	Moderate	Low	Moderate
Enterovirus	High	Long	Moderate	High
Cryptosporidium	High	Long	High	High

viable/infectious at intrusion. Fig. 2 shows processes in a pipe during wastewater intrusion into the DWDN. Chlorine decay is modeled in both the bulk water and near the pipe wall. In the bulk phase, chlorine reacts with SRA at DWDN entry points. From the intrusion point (in the DWDN), it reacts with both FRA and SRA, causing bulk chlorine decay. In the wall phase, chlorine reacts with the biofilm on the network pipe walls, leading to further chlorine decay. The equation for bulk and wall chlorine decay is described as:

$$\frac{dC_{Cl}}{dt} = f_{Cb}(C_{FRA}, C_{SRA}, C_{Cl}) + f_{Cw}(C_{Cl}) \quad 5$$

where C_{Cl} is the total chlorine concentration (mg/L) at time t (time notation omitted for simplicity), $f_{C_b}(\cdot)$ and $f_{C_w}(\cdot)$ are functions describing chlorine (mg/L) reactions in the bulk and wall phase respectively. The reaction of chlorine with FRA, SRA, and pathogens P, results in the degradation of the first two, and the inactivation of the latter.

The proposed model was applied on a real network, on which the L-Town benchmark was based. The parameters of chlorine decay (see following sections) were calibrated using real chlorine measurements from sensors installed in that network. Parameters that could not be validated from the calibration process, were based on the literature. More details on the calibration process are provided in the following sections and in the supplementary material.

2.6.1. Bulk chlorine decay

The parallel second-order model is commonly used for bulk chlorine decay, accounting for fast and slow reactions with reactants (Monteiro et al., 2014; Fisher et al., 2017a). In the fast phase, chlorine reacts with inorganic compounds and highly reactive organic compounds, represented as FRA. In the slow phase, it is consumed by less reactive organic compounds, modeled as SRA. Chlorine's reactions with pathogens are insignificant compared to those with FRA and SRA, thus they're neglected. The two-phase equation is shown below:

$$f_{Cb}(C_{FRA}, C_{SRA}, C_{Cl}) = -k_{\mathrm{FRA}} C_{\mathrm{FRA}} C_{Cl} - k_{\mathrm{SRA}} C_{\mathrm{SRA}} C_{Cl} \quad 6$$

Where k_{FRA}, k_{SRA} (L/mgh) are the decay rate coefficients for fast and slow reactions respectively.

We adopted chlorine decay parameter values from Monteiro et al. (2014) as they also examined chlorine decay in a DWDN under similar conditions of water temperature, organic material, and chlorine levels to our contamination scenario. For the value of slow reaction decay rate coefficient (k_{SRA}), we verified that the predicted values of chlorine concentration aligned with the observed sensor data. The high value of fast reaction decay rate coefficient (k_{FRA}) reported by Monteiro et al. (2014) is assumed to be suitable for our model, since high concentrations of ammonia and other inorganic compounds are expected in wastewater.

2.6.2. Wall chlorine decay

We followed the work of Monteiro et al. (2020) where the authors used the EXPBIO wall decay model by Fisher et al. (2017b) to study chlorine decay from biofilm activity in a full-scale DWDN, using first-order kinetics:

$$f_{Cw}(C_{Cl}) = -\frac{4}{D}\left(\frac{Ae^{-BC_{Cl}}}{1 + Ae^{-BC_{Cl}}/(km)} C_{Cl}\right) \quad 7$$

where D is the pipe diameter (dm), km the mass transfer coefficient (dm/h), A an amplification factor (dm/h), and finally B the rate coefficient (L/mg).

In the real network (the basis of L-Town), six chlorine sensors were installed to record chlorine concentrations at 5-min intervals. To calibrate the proposed water quality model, the network with calibrated hydraulics and known chlorine input was first simulated for one week. The wall decay parameters A and B were then adjusted to minimize the error between the model predictions and actual measurements from the chlorine sensors and ensure that the simulated chlorine residual closely resembles reality. After calibration, the parameter B was held constant at 14 (L/mg) while the A value ranged between $[0.01, 1]$, as it is related to the pipe material. Specifically, we linked A values to pipe roughness, since it is expected to correlate with the level of biofilm formation (Douterelo et al., 2016). The amount of biofilm differs across pipes, with areas that have high biofilm thickness exhibiting high chlorine demand, and areas with low thickness having lower chlorine demand. PVC pipes with roughness coefficient > 140 (Hazen-Williams), less prone to biofilm, got $A = 0.01$. Cast/galvanized iron pipes with roughness < 140, more prone to biofilm formation and wall chlorine decay, got A values between $[0.01, 1]$, with $A \in R$.

2.6.3. CRA degradation

A CRA concentration of 140 mg/L based on TOC concentration in wastewater was taken from (Metcalf et al., 1991), representing all

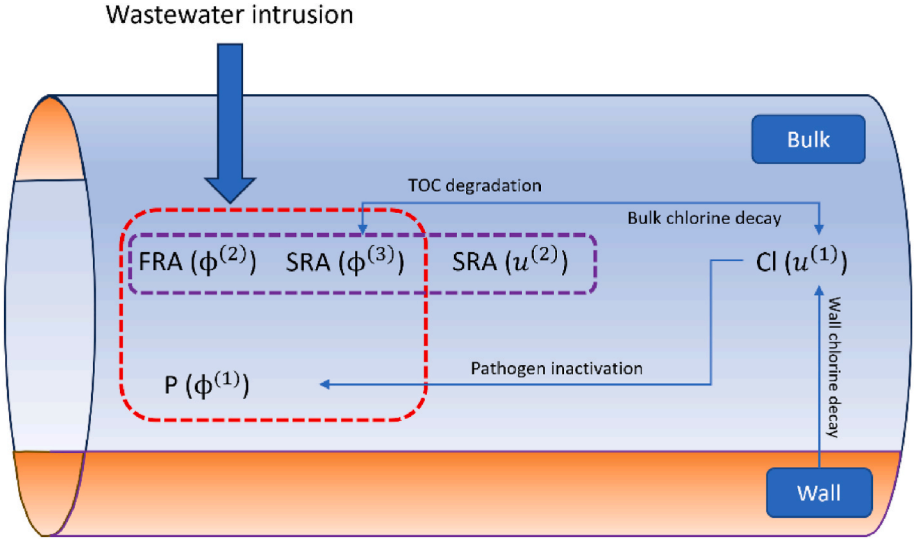

Fig. 2. Schematic showing processes during wastewater intrusion. P ($\phi^{(1)}$), FRA ($\phi^{(2)}$) and SRA ($\phi^{(3)}$) are the pathogens, the fast and the slow chlorine-reducing agents respectively entering from wastewater intrusion. Cl ($u^{(1)}$) and SRA ($u^{(2)}$) are the controlled chlorine input and the slow reducing agents respectively entering through entry points.

chlorine-reducing agents. Based on Fisher et al. (2017a), the concentrations of chlorine-reducing agents that react fast (FRA) is approximately 40% of the total chlorine-reducing agents' concentration (expressed as mgCl-equiv/L) while SRA constitute around 60%. Similarly, in the paper of Vieira et al. (2004), chlorine decay follows a similar 40%–60% pattern, indicating that the fraction of chlorine that reacts fast is approximately 40%, while the rest is 60%. This approximation serves as a practical baseline for modeling the reactive fractions of CRA. To estimate the amount of CRA entering the DWDN at its entry points, we used the SRA concentration from Monteiro et al. (2014). This refers to the CRA naturally present in the DWDN. The formula that describes the degradation of FRA and SRA is given by Monteiro et al. (2014):

$$\frac{dC_{\mathrm{FRA}}}{dt} = -k_{\mathrm{FRA}} C_{\mathrm{FRA}} C_{Cl} \tag{9}$$

$$\frac{dC_{\mathrm{SRA}}}{dt} = -k_{\mathrm{SRA}} C_{\mathrm{SRA}} C_{Cl} \tag{10}$$

2.6.4. Pathogen inactivation

Pathogen inactivation by chlorine is commonly modeled as Chick Watson kinetics (Teunis et al., 2010; Betanzo et al., 2008):

$$\frac{dC_P}{dt} = -k_p(T) C_P C_{Cl} \tag{11}$$

where C_P is pathogen concentration (CFU or PFU or oocysts/L) at time t (time notation omitted for simplicity), $k_p(T)$ is the temperature-dependent inactivation rate (L/mg h), and T is the temperature in degrees Celcius. The inactivation rate for *Campylobacter* was taken from Betanzo et al. (2008), as they also modeled microbial intrusion in a chlorinated network. Enterovirus inactivation rates were derived from Rachmadi et al. (2020), who studied chlorine inactivation of coxsackie virus, using the rate calculated from required CT values of 4 log inactivation at 5 °C.

2.6.4.1. Temperature dependence.

Using the Arrhenius equation, we defined the pathogen inactivation rate $k_p(T)$ for enterovirus and *Campylobacter* at a given temperature:

$$k_p(T) = Ae^{(-Ea/R(T+273))} \tag{12}$$

where A is the frequency factor (L/mg h), E_a the activation energy (J/mol), and R the gas constant (J/K mol). For *Cryptosporidium*, we assumed a zero inactivation rate due to its chlorine resilience. We used

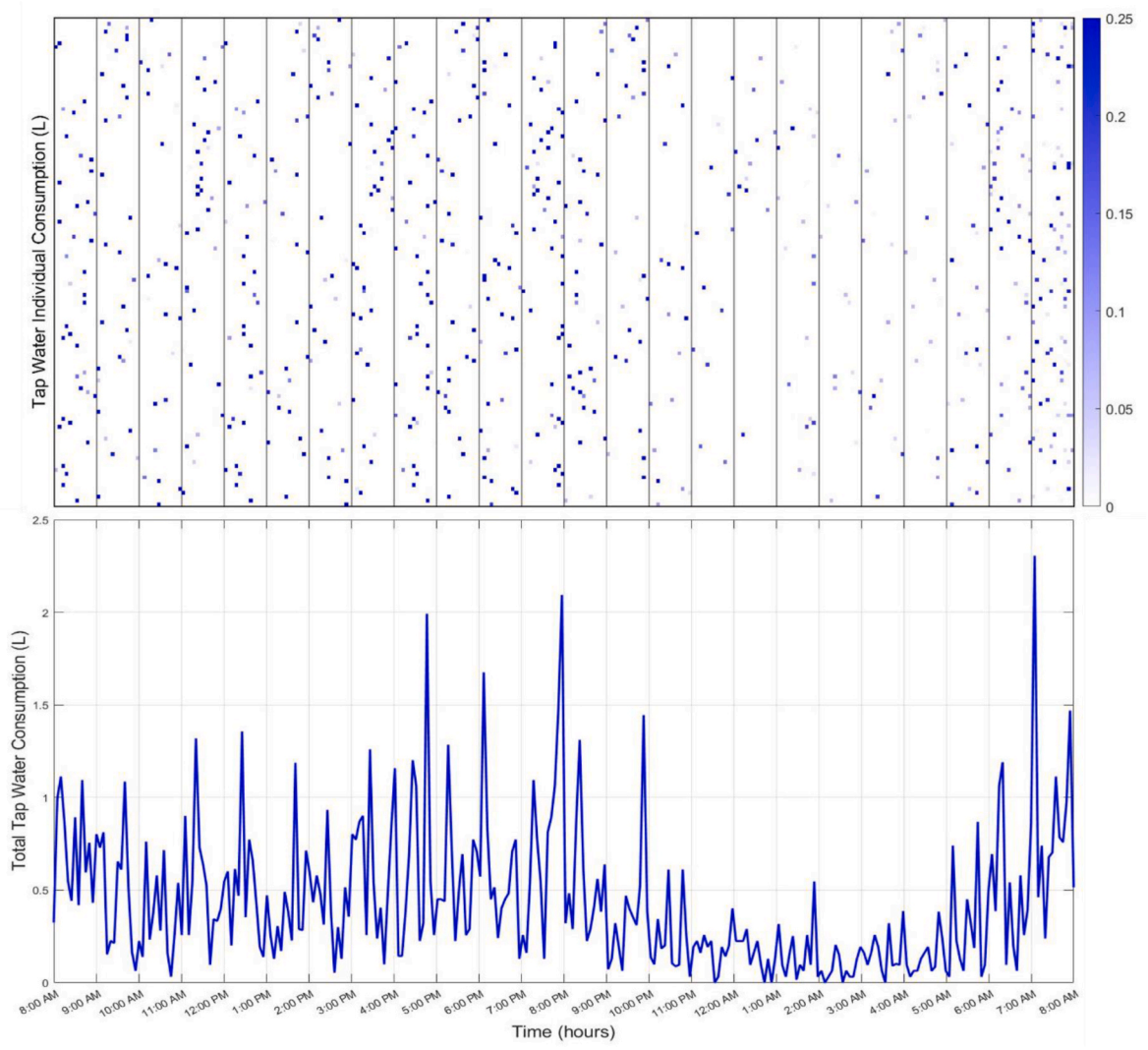

Fig. 3. The individual daily tap water consumption and the total tap water consumption for a specific node in L-Town. Each rectangle in the heatmap represents an individual consumption event, while the color indicates the volume of water consumed. (For interpretation of the references to color in this figure legend, the reader is referred to the Web version of this article.)

inactivation rates at two different temperatures to calculate A and E (Betanzo et al., 2008; Rachmadi et al., 2020).

3. Quantitative Microbial Risk Assessment

3.1. Exposure assessment

We assume that exposure to pathogens occurs only through the ingestion of tap water. We also assume that an individual person consumes 1 L of drinking water per day, divided into several consumption (exposure) events of 0.25 L or less. From all the end-uses generated by the stochastic demand generator, we isolated the tap water end-use (faucet), and considered the opening of the kitchen tap as the event that people drink water. Fig. 3 illustrates an example of multiple daily consumption events by 126 individuals in a node, where each rectangle represents an individual consumption event, while the color indicates the volume of water consumed. The plot shows the cumulative tap water consumption for the day. From this, the variability and distribution of tap water consumption behavior throughout the day for each individual is evident. Some individuals drink 1 L using only four consumption events, while others use six or seven consumption events. This variability reflects the different levels of exposure of each individual throughout the day. Pathogens ingested per consumption event are found by multiplying consumed water volume with pathogen concentration at each timestep. The daily dose per individual sums up the number of pathogens from all daily consumption events.

3.2. Health effects assessment

Each pathogen is characterized by a unique dose-response, reflecting their individual levels of infectivity. Dose response of enterovirus (coxsackie) is commonly calculated with an exponential model utilizing a value of 0.14772 for the probability of microorganism survival r (Chigor et al., 2014). For *Campylobacter* and *Cryptosporidium*, we follow Teunis et al. (2018) and Sterk et al. (2016), using the Beta-Poisson dose-response model with the hypergeometric (1F1) function for the probability of infection from outbreak studies. The parameters α and β are 0.38 and 0.51 for *Campylobacter*, and 0.106 and 0.295 for *Cryptosporidium* respectively.

3.3. Risk characterization

Integrating exposure and health effects data, we can calculate the infection risk for a specific contamination scenario. The infection probability is first calculated per individual *ind*, at a node v_i, at each time step k, considering a number of exposure events E_{ind} for each individual. Following WHO's approach (World Health Organization, 2016), we calculate infection probability from multiple exposure events over time as follows:

$$P_{inf}(ind) = 1 - \prod_{1}^{E_{ind}} \left(1 - P_{inf}(E, ind)\right) \tag{13}$$

where $P_{inf}(ind)$ is the infection probability of a single individual over the course of the contamination scenario given E_{ind} exposure events, and $P_{inf}(E, ind)$ is the probability of infection from a single exposure event $E \in \{1, \ldots, E_{ind}\}$, derived from the dose-response function of the relevant pathogen. Note that exposure events vary per individual. The number of expected infections per node v_i is then given by the sum of probabilities of infection for each individual at the node:

$$N_{inf,i} = \sum_{ind=1}^{Pop_{(i)}} P_{inf}(ind) \tag{14}$$

The infection risk for the total population in the network, given a contamination scenario, is the ratio of the total expected infected population to the total population $Pop = \sum_{i=1}^{n_v} Pop_{(i)}$, as follows:

$$R = \frac{1}{Pop} \sum_{i=1}^{n_v} N_{inf,i} \tag{15}$$

In addition, we also evaluate the infection risk for the population at the downstream nodes of the contamination source. Let $Pop_{exp} < Pop$ be the number of individuals at contaminated nodes; then, the infection risk of the exposed population R_{exp} is:

$$R_{exp} = \frac{1}{Pop_{exp}} \sum_{i=1}^{n_v} N_{inf,i} \tag{16}$$

4. Contamination scenarios

Both chlorinated and non-chlorinated networks began the contamination at 08:00 a.m. with a temperature of 12 °C. A constant SRA injection of 1.85 mgCl-equiv/L was introduced from the entry points. The chlorinated network also received a constant chlorine injection of 0.5 mg/L from the entry points.

Initial pathogen concentrations were selected as mean values based on typical concentrations in raw wastewater assuming all culture-based data represent infectious pathogens (Pitkänen and Hänninen, 2017; Betancourt and Shulman, 2016; Betancourt, 2019). The contamination duration was set at 8 hours, with a wastewater injection rate of 100 L/h to represent large contamination, while dilution was calculated from the water flow at the node where the intrusion of wastewater was modeled.

4.1. Contamination location

The study expects contamination location to significantly impact health risks, as network nodes have varying hydraulics and affect different population levels over time (Pelekanos et al., 2021). We divided the network into three zones, choosing three contamination locations for the main scenario (Fig. 4) based on their downstream population. The first location could affect about 50% of the population (Loc-L), the second around 30% (Loc-M), and the third a smaller segment at 10% (Loc-S).

4.2. Hydraulic uncertainty

Most modeling studies simplify water network hydraulics by using nominal demands, overlooking the dynamic, uncertain nature of water demands. To address this, we vary the average (base) demand of each node randomly between ±10 % of the nominal value, and then generate a stochastically determined water demand for every node using STREaM. This procedure is reiterated 100 times generating 100 unique demand profiles for each node. The goal is to ascertain whether hydraulic uncertainty influences the model outcome for each of the three contamination locations using the pathogen *Cryptosporidium*.

4.3. Quality dynamics variability and uncertainty

Modeling quality dynamics requires considering input parameter variability or uncertainty. For both enterovirus and *Campylobacter*, various inactivation rates and concentrations exist in wastewater under different conditions. To understand the impact of these uncertainties on the model outcome, we conducted a nominal range sensitivity analysis on 1) Pathogen inactivation rate (using only lower rates as higher rates eliminate all pathogens), 2) Initial contaminant concentration (considering only the highest reported concentration), and 3) Contamination duration (ranging from 2 to 24 h). Table 2 summarizes the quality parameters and initial conditions for the contamination scenario and sensitivity analysis.

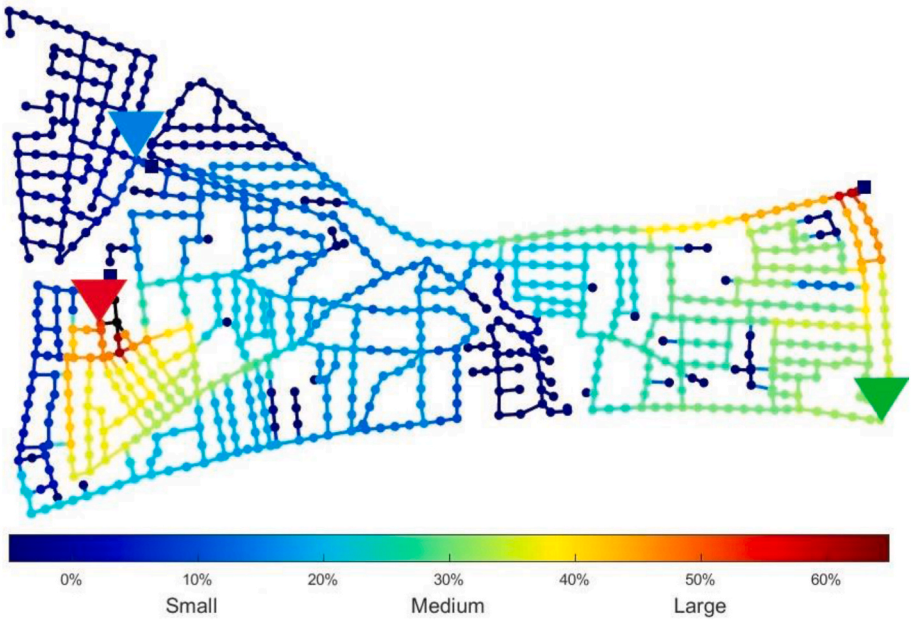

Fig. 4. The three selected contamination locations for the main scenario with small (Loc-S), medium (Loc-M) and large (Loc-L) potential impact on the population.

Table 2
Quality parameters and initial conditions incorporated into the benchmark model.

Parameter	Units	Contamination scenario	Sensitivity analysis	Notes	Reference
C_{Cl} $(u^{(1)})$	mg/L	0.5	0.5	Initial chlorine concentration	–
FRA $(\phi^{(2)})$	mgCl-equiv	$0.4CRA$	$0.4CRA$	Fast chlorine-reducing agent	Fisher et al. (2017a)
SRA $(\phi^{(3)})$	mgCl-equiv	$0.6CRA$	$0.6CRA$	Slow chlorine-reducing agent	Fisher et al. (2017a)
C_{SRA} $(u^{(2)})$	mgCl-equiv/L	$0.6CRA$	$0.6CRA$	Slow chlorine-reducing agent from reservoir	Fisher et al. (2017a)
k_{FRA}	L/mgh	0.28	0.28	decay rate coefficients for fast reactions	Monteiro et al. (2014)
k_{SRA}	L/mgh	0.007	0.007	decay rate coefficients for slow reactions	Monteiro et al. (2014)
T	Celsius	12	5 (Correlated with inactivation rate)	Temperature	–
C_{P_1} $(\phi^{(1)})$	PFU/L	$1.39e+06$	$2.08e+07$	Enterovirus initial concentration	Betancourt and Shulman (2016)
C_{P_2} $(\phi^{(1)})$	CFU/L	$9.02e+06$	$6.2e+07$	*Campylobacter* initial concentration	Pitkänen and Hänninen (2017)
C_{P_3} $(\phi^{(1)})$	oocysts/L	$3.54e+07$	$5.4e+08$	*Cryptosporidium* initial concentration	Betancourt (2019)
TOC	mg/L	140	250	TOC concentration in wastewater	Metcalf et al. (1991); Henze et al. (2002)
k_{p1}	L/mg h	92.3	-/ 19.4	Enterovirus inactivation rate	Rachmadi et al. (2020)
k_{p2}	L/mg h	265.8	-/ 157	*Campylobacter* inactivation rate	Rachmadi et al. (2020)
k_{p3}	L/mg h	0	0	*Cryptosporidium* inactivation rate	–
Duration	Hours	8	2/24	Contamination duration	–
A	dm/h	$0.01-1$	$0.01-1$	Amplification factor	–
B	L/mg	1 4	14	Rate coefficient	–
Km	Ft/h	$1.5826e-04{*}RE^{(0.58/D)}$	$1.5826e-04{*}RE^{(0.58/D)}$	Mass transfer coefficient	Shang et al. (2008b)

5. Results and discussion

5.1. Chlorinated network

Fig. 5 shows the average chlorine distribution in the L-Town network under normal operation. A chlorine concentration of 0.5 mg/L is added at the two entry points, to maintain adequate residual chlorine. While this goal is mostly achieved, a concerning area arises in the northwest where chlorine levels drop critically. This area is characterized by a flow-controlling pump that fills a tank during nighttime hours, which is then used for the morning water demand, affecting the chlorine levels.

Table 3 evaluates contamination scenarios in the chlorinated network. At the Loc-L and Loc-M locations, near the chlorinated entry points of the DWDN, chlorine residual hinders pathogen spread, resulting in fewer infections and lower infection risk for both *Campylobacter* and enterovirus.

Despite the higher *Campylobacter* concentration in wastewater compared to enterovirus (Table 2), the infection risk from enterovirus is

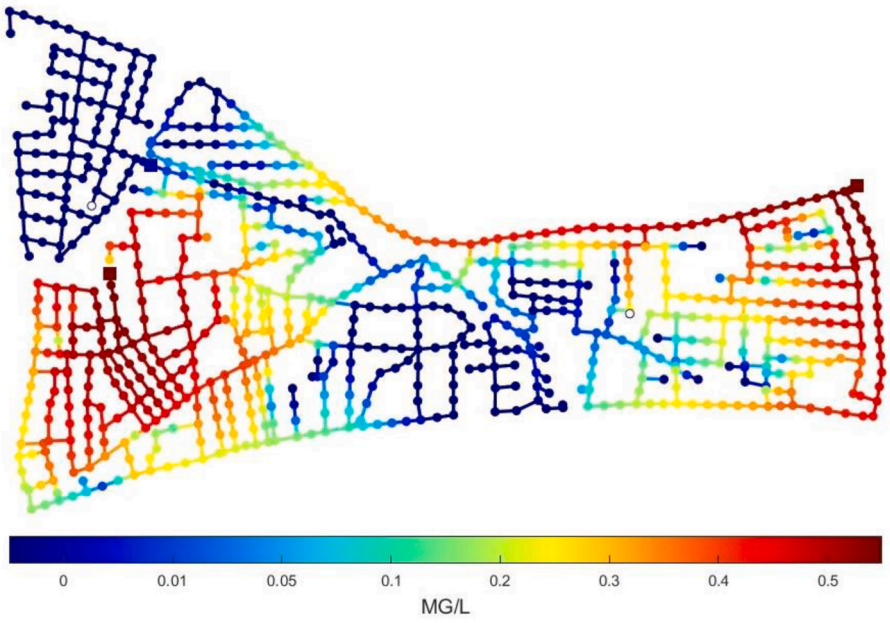

Fig. 5. The average chlorine residual in the L-Town network under normal operation.

Table 3
The results for the three pathogens in the chlorinated network. N_{inf} is the total infections, R is the infection risk for the total population, and R_{exp} is the infection risk of the downstream affected population.

Source Location	Loc-L			Loc-M			Loc-S		
Pathogens	N_{inf}	R	R_{exp}	N_{inf}	R	R_{exp}	N_{inf}	R	R_{exp}
Campylobacter	318	0.95%	2.1%	83	0.25%	0.78%	3724	11.2%	100%
Enterovirus	1158	3.5%	7.8%	2793	8.4%	26.6%	3724	11.2%	100%
Cryptosporidium	15002	45.1%	97.2%	10268	30.9%	97.9%	3705	11.1%	99.6%

higher in both Loc-L and Loc-M. This is due to *Campylobacter's* higher inactivation rate, reducing its concentration (upon chlorine reaction) more than enterovirus. This occurs even though the dose response relationship suggests that *Campylobacter* is more infectious than enterovirus when both are present at the same concentration (Fig. 6).

At the Loc-S location, low chlorine levels are due to both bulk and wall decay. Extended travel time causes more chlorine decay before chlorine reaches Loc-S. During wastewater intrusion, less dilution leads to higher FRA levels entering the network causing rapid chlorine decay. Simultaneously, less diluted pathogen concentrations increase the number of initial and surviving pathogens, raising the exposure to all pathogens downstream. This is causing higher number of infections and infection risk. Figs. S2–S7 in the supplementary material show a 24-h chlorine residual profile along with *Campylobacter* and enterovirus concentration for a node downstream of each of the three contamination locations.

Among the three pathogens, *Cryptosporidium* poses the greatest risk, showing the highest infection risk in Loc-L and Loc-M locations. This

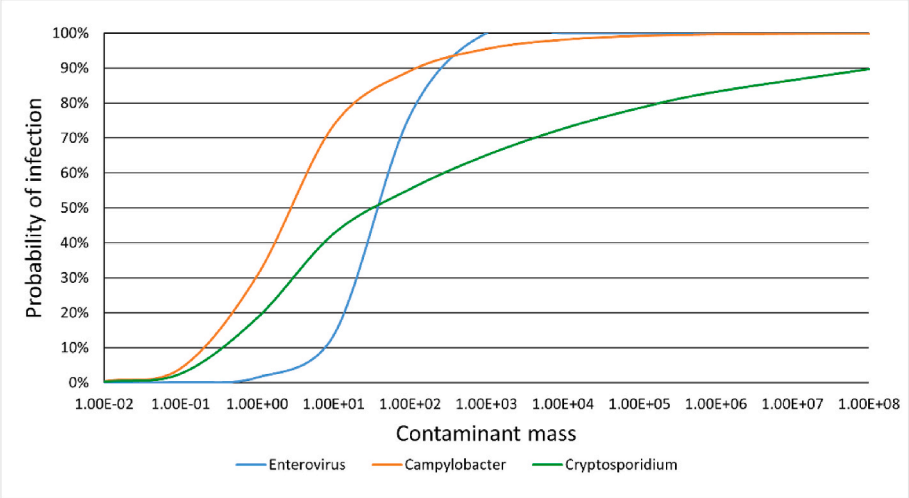

Fig. 6. The dose-response of the three reference pathogens.

elevated risk profile can be attributed to *Cryptosporidium's* resistance to chlorine disinfection, showing chlorine provides no protection against chlorine-resistant pathogens.

Fig. 7 shows the infection risk over 24 h since contamination. For pathogens *Campylobacter* and enterovirus, the infection risk primarily emerges from the Loc-S location. The identical Loc-S infection risk profiles for these two pathogens is due to their high concentrations, infecting the entire population.

The infection risk for *Cryptosporidium* differs significantly from the other two pathogens. In the Loc-L location, infection risk rapidly escalates to 25% within the first 8 hours of contamination, leveling off just above 40% by early next morning (04:00 a.m.). The rise after 04:00 a.m. is due to increased water demand as people start their (next) day, causing residual pathogens to spread and infect more individuals. The Loc-M and Loc-S locations show somewhat similar infection risks (at 15% and 10% respectively) in the first 8 hours but follow different trends. The differing risk profiles are due to variations in dilution and pathogen spread to downstream nodes. The Loc-M location, having higher dilution in certain areas and a longer path for pathogens to reach downstream nodes, experiences a gradual risk increase. Conversely, the Loc-S location has less dilution and quicker pathogen reach to downstream nodes, resulting in a more immediate surge in the infection risk. The dilution factor also influences the infection risk profile of enterovirus for Loc-L. This is due to higher contaminant dilution, as locations near the reservoir serve more downstream nodes and thus have increased flow. Consequently, the contaminant dose is reduced, leading to a lower infection risk compared to the Loc-M contamination location.

5.2. Non-chlorinated network

Table 4 shows the contamination scenario without chlorine in the network. As expected, *Campylobacter* and enterovirus present a different profile than in the chlorinated scenario, while *Cryptosporidium*'s results remain the same.

Campylobacter shows slightly more infections and higher infection risk in the Loc-L and Loc-M locations compared to enterovirus, as seen in Fig. 8. Although *Campylobacter* and enterovirus seem similar initially, they diverge after 7 hours. This behavior can be attributed to the initial concentration and dilution. *Campylobacter* has an initial concentration nearly 10 times higher than that of enterovirus, resulting in higher doses in the dose-response (Fig. 6). Regarding dilution, it takes approximately 7 hours for the contaminated plume to mix with clean water originating from the network's east side. After this interplay, dilution occurs, which reduces the dose. Referring to Fig. 6, it is evident that when the dose shifts to the left, the probability of infection from *Campylobacter* exceeds that of enterovirus at the same dose.

5.3. Hydraulic uncertainty

Fig. 9 presents the temporal progression of the infection risk over a 24-h period for the pathogen *Cryptosporidium*, as analyzed across 100 hydraulic scenarios. The influence of hydraulic uncertainty on the estimated infection risk is highlighted in all three locations. Specifically, both the Loc-L and Loc-M locations show approximately 3% variability, whereas the Loc-S location's variability remains under 1%. This 3 % variability represents a difference of about 1000 infections. Had we incorporated a larger degree of population uncertainty before calculating water demand we expect to have seen more variability.

5.4. Nominal range sensitivity analysis

Fig. 10 shows the infection risk profile of *Campylobacter* and enterovirus in the Loc-L location for the 3 parameters of the sensitivity analysis. Table S1 in the supplementary material presents the sensitivity analysis outcomes for all three locations.

The reason the two pathogens have different impactful parameters is due to their inherent characteristics in the initial contamination scenario. For example, at the Loc-L location, despite high initial

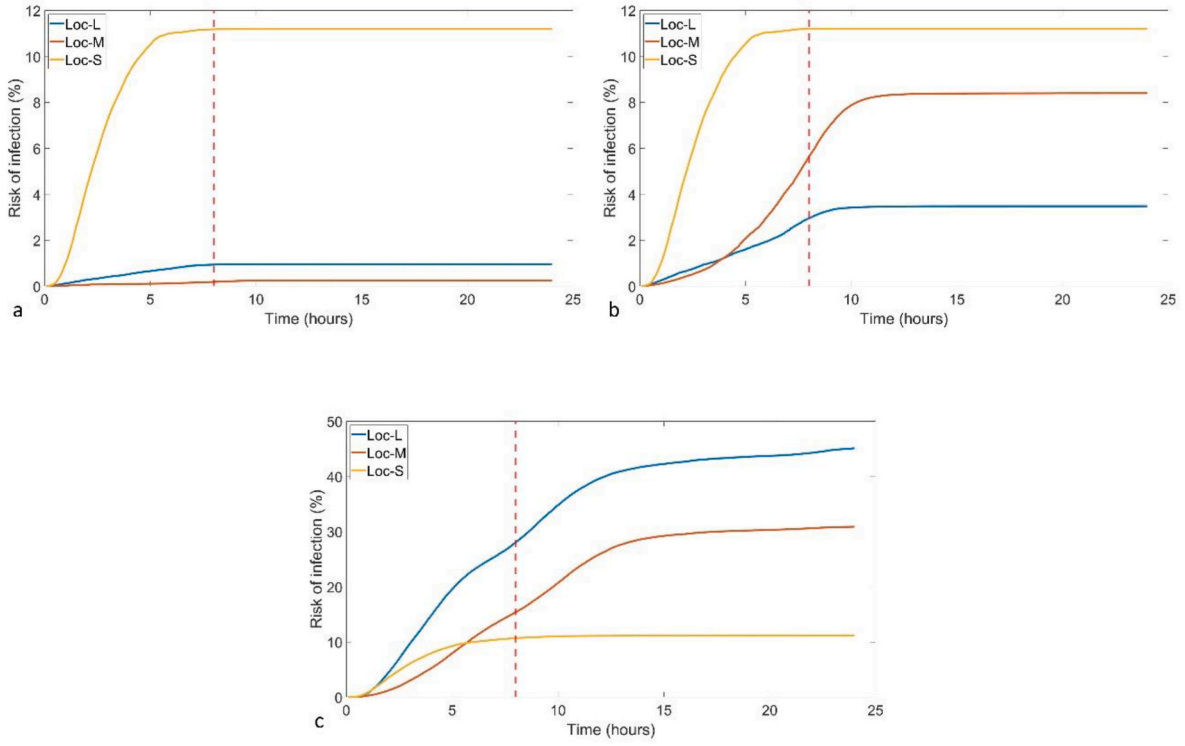

Fig. 7. The distribution of the infection risk in the chlorinated network for pathogens Campylobacter (a), enterovirus (b) and Cryptosporidium (c). The dashed red line indicates the end of the contamination. (For interpretation of the references to color in this figure legend, the reader is referred to the Web version of this article.)

Table 4
The results for the three pathogens in the non-chlorinated network. N_{inf} is the total infections, R is the infection risk for the total population, R_{exp} is the infection risk of the downstream affected population.

Source Location	Loc-L			Loc-M			Loc-S		
Pathogens	N_{inf}	R	R_{exp}	N_{inf}	R	R_{exp}	N_{inf}	R	R_{exp}
Campylobacter	15439	46.4%	100%	10467	31.45%	99.7%	3724	11.2%	100%
Enterovirus	15041	45.2%	97.4%	10304	31%	98.2%	3724	11.2%	100%
Cryptosporidium	15002	45.1%	97.2%	10268	30.86%	97.9%	3705	11.13%	99.6%

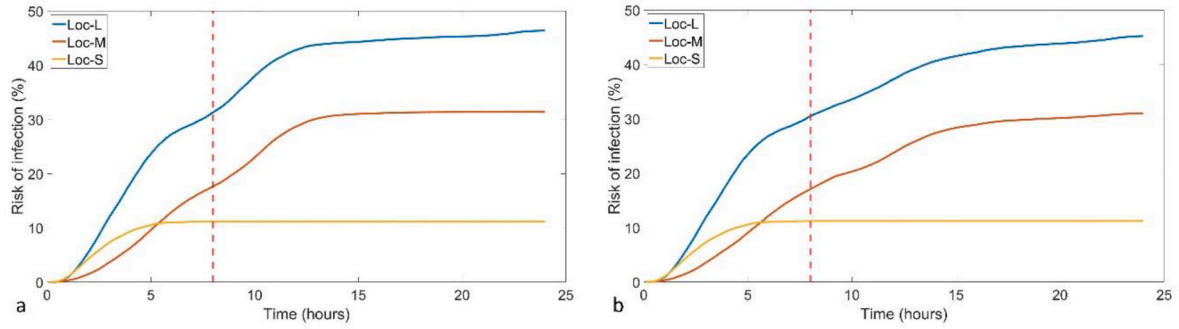

Fig. 8. The distribution of pathogens Campylobacter (a), enterovirus (b) depicting the infection risk in the non-chlorinated network. The dashed red line indicates the end of the contamination. (For interpretation of the references to color in this figure legend, the reader is referred to the Web version of this article.)

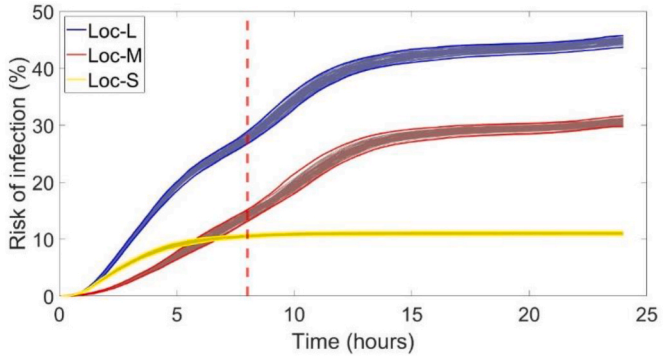

Fig. 9. Progression of the infection risk through a 24-h period for the 100 hydraulic profiles. The dashed red line indicates the end of the 8-h contamination. (For interpretation of the references to color in this figure legend, the reader is referred to the Web version of this article.)

Campylobacter concentration, chlorine's quick inactivation leads to a lower dose, thus lower infection probability as shown in Fig. 6. However, when the initial concentration increases even more, so does the dose and infection probability, putting a larger population at risk and leading to a significant rise in infection risk. For enterovirus, although subjected to chlorine inactivation in the original scenario, it caused more infections than *Campylobacter* due to its slower inactivation rate. A further decrease in this rate allows more contaminants into the network, substantially increasing the infection risk. Recognizing the potential variability of these parameters is crucial. Pathogen concentrations in wastewater vary, contamination events can last varying durations, and factors like temperature affect pathogen inactivation rates.

5.5. Role of chlorination

The results of the contamination scenarios emphasize chlorine's role in controlling waterborne pathogens in DWDN. With adequate chlorine residual, the spread of *Campylobacter* and enterovirus is greatly reduced, irrespective of contamination location as the infection risk for downstream population is only 0.78 –26.6 %. However, areas far from chlorination points may lack sufficient residual chlorine. In wastewater contamination, pathogens, especially viruses with low inactivation rates, pose a notable risk. Chlorine-resistant pathogens like *Cryptosporidium also* present a threat. This demonstrates the need for a prompt

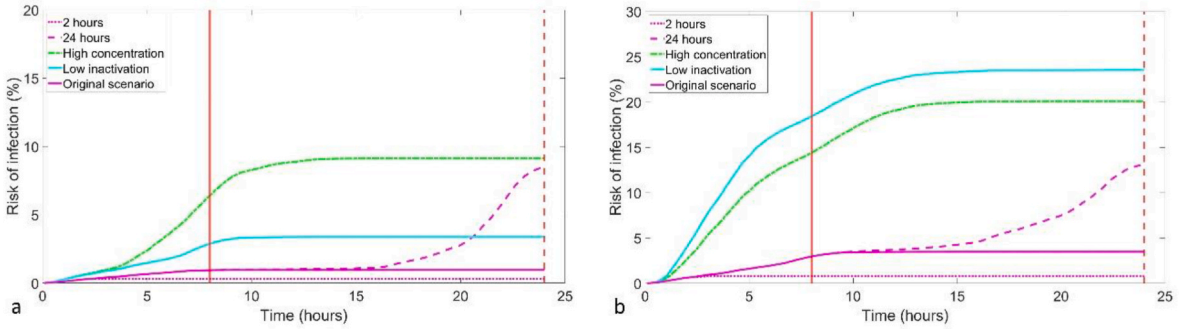

Fig. 10. The sensitivity analysis infection risk of Campylobacter (a) and enterovirus (b) in the Loc-L location. The solid and dashed red line indicate the end of the 8-h and 24-h contamination respectively. We see that Campylobacter's infection risk is more sensitive to the initial high concentration, while enterovirus, to the low inactivation rate. (For interpretation of the references to color in this figure legend, the reader is referred to the Web version of this article.)

response to such events, as within 5 – 10 hours post-contamination, 10 – 35% of the entire population could be infected.

Exploring a non-chlorinated network offers a contrasting image, where the infection risk escalates, specifically with pathogens like *Campylobacter* that have typically high concentrations in wastewater. A contamination event in a non-chlorinated network could infect 97–100% of the downstream affected population.

5.6. Role of contamination location

In both chlorinated and non-chlorinated networks, different contamination locations exhibit unique risk profiles. Contaminations in larger zones, especially in non-chlorinated networks, bear more infection risk over time due to more contaminated downstream nodes. Conversely, contaminations in smaller zones have lower infection risk but are prone to immediate risk surges due to rapid pathogen spread to downstream nodes. Dilution also matters; contamination near the reservoir may lead to more dilution, reducing the contaminant mass per node, while contamination at the network's periphery may result in less dilution and higher contaminant mass. This demonstrates how the network's structural characteristics influence the infection risk.

5.7. Limitations and recommendations

Our risk estimation relies on specific dose-response models. Using different dose-response models could alter results, showing that the computed risk is tied to the chosen dose-response model. A limitation is the study's focus on individual pathogen infection risk. Realistically, wastewater carries multiple pathogens at different concentrations. Future work should explore cumulative infection risk, considering the dose response of all pathogens together for a holistic infection risk assessment, especially in networks with low to no chlorine residual.

One form of limitation is the assumption that exposure to pathogens occurs only through kitchen tap water ingestion since exposure can also happen via showering, brushing teeth. Although our proposed methodology for the distribution of daily tap water consumption provides adequate variability of drinking water consumption over time as evidenced in Fig. 3, exploring variability of individual consumption volumes of tap water (e.g. 0, 0.2, 0.5, 2, 3 or 4 L/p/d) could capture even more variability in individual water consumption behavior.

Another limitation is the absence of real data for CRA concentrations in wastewater. Our analysis uses approximations made in the literature that considers TOC concentration as representative of CRA, assuming chlorine mainly interacts with inorganic substances (and some organic) during the fast phase, and mainly organics in the slow phase.

The calibration of the BeWaRE testbed was carried out using network-specific data that enhanced the accuracy of a model. Several components of the BeWaRE testbed are transferable and can be applied to different networks (with different types of water systems), e.g., the water quality model component, or the QMRA component. However, if water utilities want to use those components in their network, they would first need to calibrate the parameters to get realistic results.

5.8. Operational changes in water management and policy

The proposed model can potentially influence operational changes in water management since it emphasizes the necessity of advanced modeling tools to effectively mitigate pathogen contamination events in the DWDN. Not many people are exposed to incidents but when they are affected by an incident, their exposure to pathogens (or infection risk) is high and there is a small window of opportunity for meaningful interventions. We believe that our tool can also influence policy. Once again, the results of our contamination scenario highlight the need to integrate Water Security Plans into existing Water Safety Plans and to develop Standard Operating Procedures for contamination emergency responses. Finally, using such computational models to estimate (with high resolution) health impact and adopting the use of such technologies for decision support can optimize response strategies and improve system resilience.

5.9. Application to real case studies

BeWaRE has been applied to real case studies in the context of the EU-funded PathoCERT (Pathogen Contamination Emergency Response Technologies) project. The aim of the project was to enhance the coordination capabilities of first responders during pathogen contamination emergencies. BeWaRE was integrated in a decision-support tool named PathoINVEST (Paraskevopoulos et al., 2022) and was applied in three European case studies, each featuring distinct characteristics. In Spain and Cyprus, it was used to assist the response to earthquakes that led to sewage infiltration into the DWDN. In the Netherlands, it was employed to investigate suspected intentional contamination following customer complaints. In each case study, emergency response teams comprising individuals from all relevant sectors (water utilities, civil protection, and health care). These teams incorporated their own network data into BeWaRE, having an accurate representation of the contaminant transport, as well as health impact analysis.

6. Conclusion

This study introduced BeWaRE, an open-access testbed, featuring an integrated hydraulic and water quality model. It includes pathogen concentration data, intrusion scenarios, chlorine (decay) effects, stochastic water demands and tap water end-use within a QMRA framework. We demonstrated its applicability by analyzing health implications from wastewater contamination in a DWDN, and chlorination's role in mitigating risks from different enteric pathogens. Key findings include:

- In non-chlorinated DWDN, the modeled wastewater contamination events led to 11–46% infection risk in the total population, depending on the contamination location, but irrespective of the selected pathogen (due to the high pathogen concentration).
- In chlorinated DWDN, the same scenarios resulted in lower infection risk for the pathogens that are susceptible to chlorine; 0.78 – 2.1% for *Campylobacter* and 7.8 – 26.6% for enterovirus. Enterovirus infection risk is higher, despite the concentrations in the contamination source being lower, due to the lower susceptibility to chlorine than *Campylobacter*.
- In chlorinated DWDN, the modeled contamination scenarios yielded infections as a result of Cryptosporidium, due to its high chlorine resistance. Contamination location plays a significant role in terms of impact, due to the size of the affected population, but also due to the level of dilution of the contamination in the DWDN.
- The response window after a contamination event to reduce the health impact a is short; in these scenarios 5 – 10 hours post-contamination.
- *Campylobacter's* infection risk is more sensitive to the initial concentration in the contamination source whereas enterovirus infection risk to inactivation rate.

This testbed can serve as a baseline for future studies, potentially exploring different inactivation kinetics, alternative pathogens, varied water consumption patterns, or calibrating the model for real-world drinking water systems. This study illuminates the profound health implications of a large wastewater contamination in drinking water networks. While chlorination plays an essential defensive role, a comprehensive understanding of pathogen behavior is crucial for enhancing protection against potential outbreaks and ensuring a safer water supply.

CRediT authorship contribution statement

Sotirios Paraskevopoulos: Writing – review & editing, Writing – original draft, Visualization, Software, Methodology, Investigation, Formal analysis, Data curation, Conceptualization. **Stelios Vrachimis:** Writing – review & editing, Writing – original draft, Methodology, Formal analysis, Data curation. **Marios Kyriakou:** Visualization, Software, Data curation, Conceptualization. **Demetrios G. Eliades:** Writing – review & editing, Validation, Supervision, Investigation, Funding acquisition, Conceptualization. **Patrick Smeets:** Writing – review & editing, Validation, Supervision, Methodology. **Marios Polycarpou:** Writing – review & editing, Validation, Supervision, Funding acquisition, Conceptualization. **Gertjan Medema:** Writing – review & editing, Validation, Supervision, Funding acquisition, Conceptualization.

Declaration of competing interest

The authors declare that they have no known competing financial interests or personal relationships that could have appeared to influence the work reported in this paper.

Acknowledgements

This project has received funding from the European Union's Horizon 2020 research and innovation programme under grant agreement No. 883484 (PathoCERT), the European Research Council (ERC), under the ERC Synergy grant agreement No. 951424 (Water Futures), and was supported by the European Union's Horizon 2020 Teaming programme under grant agreement No. 739551 (KIOS CoE), and the Government of the Republic of Cyprus through the Deputy Ministry of Research, Innovation and Digital Policy.

Appendix A. Supplementary data

Supplementary data to this article can be found online at https://doi.org/10.1016/j.jclepro.2024.143997.

Data availability

The code associated with the presented research can be found in: Wastewater contamination https://doi.org/10.5281/zenodo.10171279

References

Abhijith, G.R., Ostfeld, A., 2021. Modeling the response of nonchlorinated, chlorinated, and chloraminated water distribution systems toward arsenic contamination. J. Environ. Eng. 147 (10), 04021045.
Betancourt, W., 2019. Cryptosporidium Spp.
Betancourt, W.Q., Shulman, L.M., 2016. Polioviruses and other enteroviruses. In: Rose, J. B., Jiménez-Cisneros, B. (Eds.), Global Water Pathogen Project.
Betanzo, E.W., Hofmann, R., Hu, Z., Baribeau, H., Alam, Z., 2008. Modeling the impact of microbial intrusion on secondary disinfection in a drinking water distribution system. J. Environ. Eng. 134 (4), 231–237.
Blokker, M., Smeets, P., Medema, G., 2018. Quantitative microbial risk assessment of repairs of the drinking water distribution system. Microbial Risk Analysis 8, 22–31.
Boulos, P.F., Lansey, K.E., Karney, B.W., 2006. Comprehensive Water Distribution Systems Analysis Handbook for Engineers and Planners. American Water Works Association.
Chigor, V.N., Sibanda, T., Okoh, A.I., 2014. Assessment of the risks for human health of adenoviruses, hepatitis A virus, rotaviruses and enteroviruses in the Buffalo River and three source water dams in the Eastern Cape. Food and Environmental Virology 6, 87–98.
Clark, R.M., Yang, Y.J., Impellitteri, C.A., Haught, R.C., Schupp, D.A., Panguluri, S., Krishnan, E.R., 2010. Chlorine fate and transport in distribution systems: experimental and modeling studies. J. Am. Water Works Assoc. 102 (5), 144–155.
Cominola, A., Giuliani, M., Castelletti, A., Rosenberg, D.E., Abdallah, A.M., 2018. Implications of data sampling resolution on water use simulation, end-use disaggregation, and demand management. Environ. Model. Software 102, 199–212.
Craun, G.F., Calderon, R.L., 2001. Waterborne disease outbreaks caused by distribution system deficiencies. J. Am. Water Works Assoc. 93 (9), 64–75.
Douterelo, I., Husband, S., Loza, V., Boxall, J., 2016. Dynamics of biofilm regrowth in drinking water distribution systems. Appl. Environ. Microbiol. 82 (14), 4155–4168.
Eliades, D.G., Kyriakou, M., Vrachimis, S., Polycarpou, M.M., 2016. EPANET-MATLAB toolkit: an open-source software for interfacing EPANET with MATLAB. In: Proc. 14th International Conference on Computing and Control for the Water Industry (Ccwi), vol. 8.
Eliades, D.G., Vrachimis, S.G., Moghaddam, A., Tzortzis, I., Polycarpou, M.M., 2023. Contamination event diagnosis in drinking water networks: a review. Annu. Rev. Control 55, 420–441.
Fisher, I., Kastl, G., Sathasivan, A., 2017a. A comprehensive bulk chlorine decay model for simulating residuals in water distribution systems. Urban Water J. 14 (4), 361–368.
Fisher, I., Kastl, G., Sathasivan, A., 2017b. New model of chlorine-wall reaction for simulating chlorine concentration in drinking water distribution systems. Water Res. 125, 427–437.
Frankel, M., Katz, L.E., Kinney, K., Werth, C.J., Zigler, C., Sela, L., 2023. A framework for assessing uncertainty of drinking water quality in distribution networks with application to monochloramine decay. J. Clean. Prod. 407, 137056.
Giammanco, G.M., Bonura, F., Urone, N., Purpari, G., Cuccia, M., Pepe, A., et al., 2018. Waterborne Norovirus outbreak at a seaside resort likely originating from municipal water distribution system failure. Epidemiol. Infect. 146 (7), 879–887.
Henze, M., Harremoes, P., Jansen, J.L., Arvin, E., 2002. Wastewater Treatment: Biological and Chemical Process. Springer-Verlag.
Hrudey, S.E., Hrudey, E.J., 2004. Safe Drinking Water. IWA publishing.
Hrudey, S.E., Hrudey, E.J., 2019. Common themes contributing to recent drinking water disease outbreaks in affluent nations. Water Supply 19 (6), 1767–1777.
Kuhn, K.G., Falkenhorst, G., Emborg, H.D., Ceper, T., Torpdahl, M., Krogfelt, K.A., et al., 2017. Epidemiological and serological investigation of a waterborne Campylobacter jejuni outbreak in a Danish town. Epidemiol. Infect. 145 (4), 701–709.
Laine, J., Huovinen, E., Virtanen, M.J., Snellman, M., Lumio, J., Ruutu, P., et al., 2011. An extensive gastroenteritis outbreak after drinking-water contamination by sewage effluent, Finland. Epidemiol. Infect. 139 (7), 1105–1113.
LeChevallier, M.W., 1999. The case for maintaining a disinfectant residual. J. Am. Water Works Assoc. 91 (1), 86–94.
Medema, G.J., Smeets, P.W.M.H., Van Blokker, E.J.M., Lieverloo, J.H.M., 2013. Safe distribution without a disinfectant residual. Microbial Growth in Drinking-Water Supplies. Problems, Causes, Control and Research Needs 95–125.
Metcalf, L., Eddy, H.P., Tchobanoglous, G., 1991. Wastewater Engineering: Treatment, Disposal, and Reuse, vol. 4. McGraw-Hill, New York.
Monteiro, L., Carneiro, J., Covas, D.I., 2020. Modelling chlorine wall decay in a full-scale water supply system. Urban Water J. 17 (8), 754–762.
Monteiro, L., Figueiredo, D., Dias, S., Freitas, R., Covas, D., Menaia, J., Coelho, S.T., 2014. Modeling of chlorine decay in drinking water supply systems using EPANET MSX. Procedia Eng. 70, 1192–1200.
Odhiambo, M., Viñas, V., Sokolova, E., Pettersson, T.J., 2023. Health risks due to intrusion into the drinking water distribution network: hydraulic modelling and quantitative microbial risk assessment. Environ. Sci. J. Integr. Environ. Res.: Water Research & Technology 9 (6), 1701–1716.
Paraskevopoulos, S., Vrachimis, S., Kyriakou, M., Pavlou, P., Kouzapas, D., Milis, G., Smeets, P., Eliades, D., Medema, G., Polycarpou, M., Panayiotou, C., 2022. PathoINVEST: pathogen contamination investigations during emergencies. In: 2nd International Joint Conference on Water Distribution Systems Analysis & Computing and Control in the Water Indsustry. Universitat Politecnica de Valencia. https://doi.org/10.4995/WDSA-CCWI2022.2022.14799.
Pelekanos, N., Nikolopoulos, D., Makropoulos, C., 2021. Simulation and vulnerability assessment of water distribution networks under deliberate contamination attacks. Urban Water J. 18 (4), 209–222.
Pitkänen, T., Hänninen, M.L., 2017. Members of the family Campylobacteraceae: Campylobacter jejuni, Campylobacter coli. Global Water Pathogens Project. http://www.waterpathogens.org.
Rachmadi, A.T., Kitajima, M., Kato, T., Kato, H., Okabe, S., Sano, D., 2020. Required chlorination doses to fulfill the credit value for disinfection of enteric viruses in water: a critical review. Environ. Sci. Technol. 54 (4), 2068–2077.
Rossman, L.A., 2000. EPANET 2: Users Manual.
Shang, F., Uber, J.G., Rossman, L.A., 2008a. Modeling reaction and transport of multiple species in water distribution systems. Environ. Sci. Technol. 42 (3), 808–814.
Shang, F., Uber, J.G., Rossman, L.A., Janke, R., 2008b. EPANET multi-species extension user's manual. Risk Reduction Engineering Laboratory. US Environmental Protection Agency, Cincinnati, Ohio.
Sterk, A., Schijven, J., de Roda Husman, A.M., de Nijs, T., 2016. Effect of climate change on runoff of Campylobacter and Cryptosporidium from land to surface water. Water Res. 95, 90–102.
Teixeira, R., Carmi, O., Raich, J., Gattinesi, P., Hohenblum, P., 2019. Guidance for Production of a Water Security Plan in Drinking Water Supply.
Teunis, P.F.M., Xu, M., Fleming, K.K., Yang, J., Moe, C.L., LeChevallier, M.W., 2010. Enteric virus infection risk from intrusion of sewage into a drinking water distribution network. Environ. Sci. Technol. 44 (22), 8561–8566.
Teunis, P.F., Marinović, A.B., Tribble, D.R., Porter, C.K., Swart, A., 2018. Acute illness from Campylobacter jejuni may require high doses while infection occurs at low doses. Epidemics 24, 1–20.
Todini, E., 1987. A gradient method for the analysis of pipe networks. In *Lnternational Conference On Computer Applications For Water Supply and Distribution*.
van Lieverloo, J.H.M., Blokker, E.M., Medema, G., 2007. Quantitative microbial risk assessment of distributed drinking water using faecal indicator incidence and concentrations. J. Water Health 5 (S1), 131–149.

Vieira, P., Coelho, S.T., Loureiro, D., 2004. Accounting for the influence of initial chlorine concentration, TOC, iron and temperature when modelling chlorine decay in water supply. J. Water Supply Res. Technol. - Aqua 53 (7), 453–467.
Vrachimis, S.G., Eliades, D.G., Taormina, R., Kapelan, Z., Ostfeld, A., Liu, S., et al., 2022. Battle of the leakage detection and isolation methods. J. Water Resour. Plann. Manag. 148 (12), 04022068.
Vrachimis, S.G., Timotheou, S., Eliades, D.G., Polycarpou, M.M., 2019. Iterative hydraulic interval state estimation for water distribution networks. J. Water Resour. Plann. Manag. 145 (1), 04018087.
World Health Organization, 2016. Quantitative Microbial Risk Assessment: Application for Water Safety Management.
World Health Organization, 2017. Guidelines for Drinking-Water Quality: First Addendum to the, fourth ed.
Yang, J., LeChevallier, M.W., Teunis, P.F., Xu, M., 2011. Managing risks from virus intrusion into water distribution systems due to pressure transients. J. Water Health 9 (2), 291–305.